Characterization of Belt Drive Systems in Hybrid Powertrains

AIAS – ASSOCIAZIONE ITALIANA PER L'ANALISI DELLE SOLLECITAZIONI

45° CONVEGNO NAZIONALE, 7-10 SETTEMBRE 2016 – UNIVERSITÀ DEGLI STUDI DI TRIESTE

AIAS 2016 - 642

CHARACTERIZATION OF BELT DRIVE SYSTEMS IN HYBRID POWERTRAINS

M. di Napoli[a], M. Straehle[b], S. Ruzimov[a],
L.D. Suarez Cabrera[a], N. Amati[a], A. Tonoli[a]

[a] *Politecnico di Torino – Dipartimento di Ingegneria Meccanica e Aerospaziale,*
Corso Duca degli Abruzzi, 24, 10129 Torino, Italia, e-mail: maria.dinapoli@polito.it
[b] *Technische Universitaet Darmstadt,*
Karolinenplatz 5, 64289 Darmstadt, Germania

Sommario

Nel presente lavoro si intende presentare l'ideazione e la realizzazione di un banco prova atto alla caratterizzazione in termini di efficienza del sistema di distribuzione a cinghia degli accessori. Lo studio è in particolare indirizzato a quei sistemi in cui viene introdotto, in luogo del tradizionale alternatore, un Belt Starter Generator (BSG). Un BSG è una macchina elettrica capace di lavorare oltre che come generatore (funzionando come un normale alternatore o durante una frenata regenerativa) anche da motore (per effettuare operazioni come l'avvio del motore o la produzione di trazione elettrica e boost). L'utilizzo di tale dispositivo si colloca nella categoria delle tecnologie "mild-hybrid", volte alla riduzione dei consumi e delle emissioni caratteristiche del funzionamento del motore a combustione interna mediante l'ausilio di macchine elettriche. L'introduzione di un BSG nel girocinghia di distribuzione comporta delle forti variazioni della tensione della cinghia causate dall'alternanza di ramo teso e ramo lasco. Lo studio dell'efficienza di tale sistema è di fondamentale importanza per la definizione della migliore strategia di funzionamento di sistemi mild-hybrid provvisiti fi giro cinghia con BSG.

Abstract

The present work is intended to describe the concept and realization of a test rig for the characterization of the efficiency of front end accessory drives. The study is in particular addressed to those systems where the traditional alternator is replaced with a Belt Starter Generator (BSG). A BSG is an electric machine capable of working both as generator (to function as traditional alternator and regenerate energy during braking) and as motor (to start the engine and provide electric traction and boosting). The utilization of such device is among the solutions adopted by mild hybrid technologies that are addressed to the reduction of fuel consumption and pollutant emissions typical of ICEs by the application of electric machines. The introduction of a BSG into a belt drive system leads to strong variations of the belt tension due to the alternation of tight and slack span. The study of the efficiency of such system is crucial in defining the best operating strategy of mild hybrid systems comprising a Belt Drive System (BDS) equipped with a BSG.

Key words: mild hybrid, belt drive system, belt starter generator, transmission efficiency, belt pretension, power losses.

1. INTRODUCTION

The automotive industry is nowadays facing increasingly strict demands for fuel consumption and pollutant emissions reduction. Traction and accessories electrification is a research topic widely discussed in recent literature. The latest trend is the development of mild-hybrid technologies that support the Internal Combustion Engine (ICE) in different operating conditions [1]. A mild-hybrid is a system where an electric machine able to work both as generator and motor is used to perform functions such as automatic ICE stop-start, launch assist, regenerative braking, and other features [2]. Two fundamental concepts for a combined starter-generator machine have been developed [3]: an Integrated Starter Generator (ISG) that is placed directly onto the crankshaft between the engine and the clutch and which replaces the fly wheel, and a Belt Driven Starter Generator (BSG) that replaces the alternator in the conventional Front End Accessory Drive (FEAD). The BSG replaces the conventional alternator with a low impact on the engine compartment layout, while the ISG solution requires a completely revised housing [1]. A FEAD provided with a BSG is therefore the less invasive and expensive solution and the most likely to be adopted by car manufacturers. Nevertheless, the installation of a BSG in a FEAD leads to excessive strain on the belt due to its severe operating conditions. The transmitted torque is inverted when the ICE drives the belt and when the belt is driven by the BSG. This results in a tight branch of the belt drive to become loose and vice versa causing large variation of belt tension [4]. The irregular stresses acting on the belt require the use of a tensioner capable of keeping the belt tension inside a safe range during operation and of preventing slippage during all the operating conditions of the drive. With this goal many solutions are currently being studied such as two tensioners one for each span, active tensioners, double arm tensioners and hydraulic tensioners.
The critical issues due to the involvement of BSG in BDS and the need for identifying the best operating strategy require a deep study focused on the tension conditions of the belt and its influence on the overall efficiency of the system.
To identify critical issues and characterize the losses of BDS under different working conditions, a test rig of BDS was realized. In order to replicate the operating conditions of a BDS two permanent magnet motors reproducing the dynamics of both the ICE and the BSG are used. A sensors and control architecture was outlined in order to obtain the complete monitoring of the fundamental parameters of the system.
The present work provides an insight into the critical issues and the power losses that can affect a proper operation of BDS and presents the main characteristics of a dedicated test rig. Additionally, the first experimental characterization performed on the test rig is described.

2. OPERATING CONDITIONS AND CRITICAL ISSUES

Belt Drive Systems usually work in the severe ambient conditions of the engine compartment and are subject to highly dynamic excitations coming from the crankshaft irregularities. This harmonic excitation together with the inertia of the accessories (mainly the alternator) and high loading conditions of the BDS (especially in ICE cold cranking, electric traction and regenerative braking), leads to vibrations of the belt and high tension fluctuations that can cause slippage and noise. In this section special attention is given to the typical operating conditions of a BDS equipped with a BSG and to the different power losses that these can lead to.

2.1. Operating modes

It is important to identify the different operating conditions that can affect the functioning of a BDS equipped with a BSG. Both the operating conditions of the ICE and of the BSG will contribute to define the dynamic excitation acting on the BDS.
For what concerns the ICE, its operating conditions are dominated by the reciprocating movements of the crankshaft (CS) and by the irregularities of the forces exerted by hot gasses on the pistons. The resulting speed imposed by the crankshaft to the BDS can be described as the sum of many harmonic components whose frequencies are multiples of the rotational speed of the machine. The resulting CS speed can be therefore described as suggested by [5] with following expression:

$$\omega_{CS} = \omega_{mean} + \sum_{n=1}^{4} A_n \cos(n\omega_{mean}t + \varphi_n) \quad (1)$$

It is clear how this fluctuations in transmitted speed will imply into BDS also high torque variations, particularly highlighted by the inertial elements composing the overall system.
A BSG either absorbs power from the BDS or powers it. Its typical operating modes can be divided into the following groups:

- Traditional alternator operation
- Regenerative braking
- Electric traction mode
- Engine start in warm and cold conditions, i.e. warm and cold cranking
- Electric boost, i.e. traction with ICE on and providing electric boost from BSG

The variations of operating conditions of ICE and BSG described above involve speed and torque irregularities that in the BDS produce power losses that cannot be neglected.

2.2. Power losses in Belt Drive Systems

According to the extensive literature about BDS, it is possible to delineate a classification of the losses that affect the transmission efficiency in belt drives according to the scheme on Fig. 1. The most general distinction is between external and internal friction losses as theorized by Gerbert [6]. These losses have been alternatively referred to as speed and torque losses respectively [7-10].

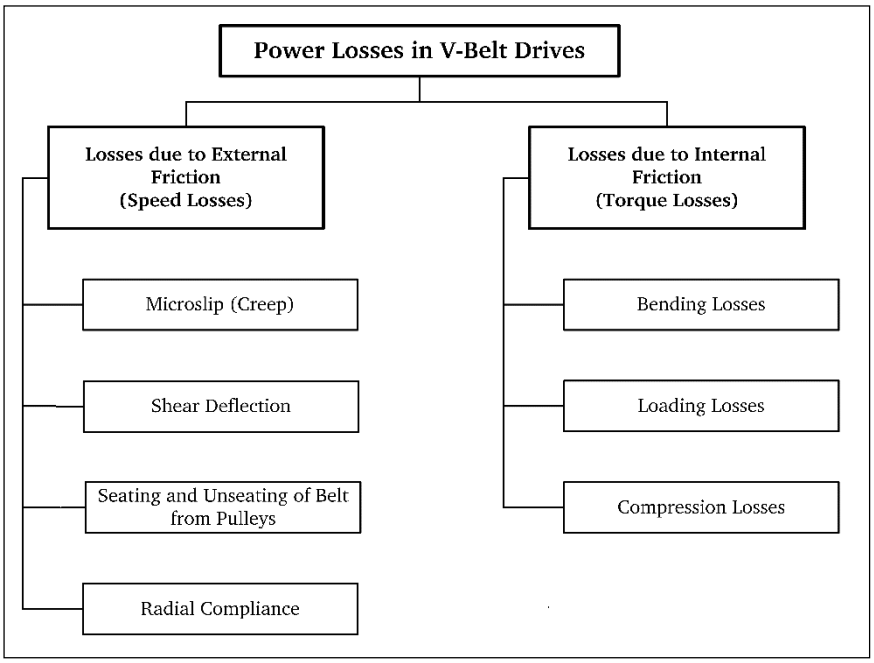

Figure 1 Power losses classification

External losses are caused by the contact mechanics between belt and pulley and result not only in a difference between the speed of the driving pulley and the speed transmitted to the driven pulley but also in a slip between the belt and the pulley surface while the belt enters and exits the pulley. According to Gerbert [11] there are four contributions to speed losses: creep along the belt, shear deflection, belt seating and unseating, radial compliance. Belt creep and shear deflection are originated by the speed differential existing between the tension member of the belt and the pulley surface. Such differential generates shear strains in the belt envelope which determine the so-called shear deflection in the arc of adhesion of the pulley, where the static friction forces provide traction. At the point where the shear strains overcome the friction forces, the slip described in the creep theory takes place. The arc of slip, also known as active arc, composes together with the arc of adhesion the total arc of contact between belt and pulley [12].

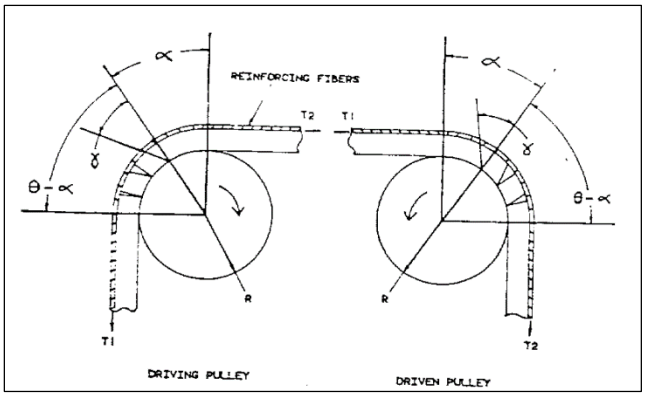

Figure 2 Arc of adhesion and arc of slip compose the arc of contact between belt and pulley [12]

Radial compliance and belt seating and unseating phenomena are originated by the possibility of a V-belt or V-ribbed belt to move radially into the pulley grooves and are directly linked to cross sectional data and material properties of the belt [13, 14]. Because of the tension difference existing on tight and slack spans, the radius at the entry and exit regions of the belt-pulley contact are not equal on driving and driven pulleys [13]. This leads directly to the radial belt compliance, as described in Fig. 2.

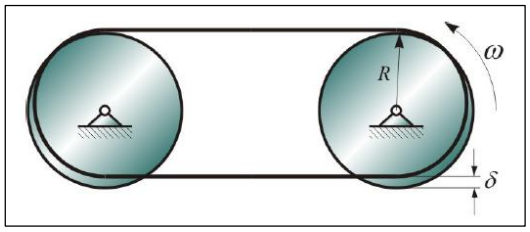

Figure 3 Radial Compliance [13]

Applying additional loads on the belt, for example activating the AC compressor or loading the alternator with high loads, the pressure variations can therefore cause radial displacements of the belt that will undergo the seating and unseating effects. As described in Fig. 3, while the unloaded belt fits the pulley at a reference radius (R), the force (F) on the belt causes a displacement (x) and fits the belt in the pulley groove at a radius (r) [14].

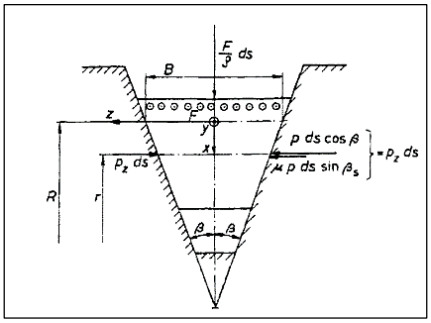

Figure 4 Radial displacement description [14]

Internal losses, or torque losses, are due to the hysteresis of the belt material. Losses due to internal friction (hysteresis) in the materials which compose the belt (reinforcing cord, rubber layer and cover) occur when the belt is bent around the pulley (bending losses), stretched due to power transmission (loading losses) and compressed into the pulley groove (compression losses). Hysteresis losses can be additionally divided into losses due to longitudinal and lateral deformation, as suggested by [15].

3. EXPERIMENTAL SETUP AND TEST RIG CHARACTERISTICS

The critical issues highlighted require an experimental analysis focused on BDS and its overall efficiency in relation to its different operating conditions. In this context, a test rig was developed to allow the study of BDS dynamics and power loss characteristics. The test rig is shown in Figure 5 and it mounts two electric motors to simulate BSG and ICE behavior. This choice was taken to obtain major advantages over the utilization of traditional engine cells. Measurements obtained in such testing environments have a high level of uncertainty due to the uncontrollable irregularities that characterize the physical phenomena occurring into the ICE. The designed test rig allows the reproduction of a realistic and controllable testing environment. The use of two electric motors for the dynamic simulation of the BSG and the crankshaft of the ICE allows reproducing the different operating conditions of the BDS. In addition, it is fundamental for taking into account the crankshaft oscillations due to the overlapping of the harmonics. The harmonics are generated via the Electronic Control Unit (ECU) in a predictable and repeatable manner.
The design was performed to obtain the maximum versatility and allow the test rig reproducing different kind of BDS, both for what the mounting solutions and the characteristic of the components are concerned. The aim of the present section is to give an overview of the test rig and illustrate its main characteristics.

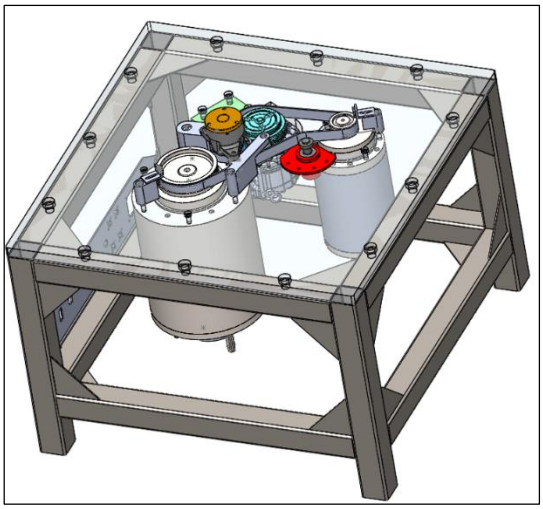

Figure 5 3D assembly of the designed test rig

3.1. Mechanical layout

Fig. 5 shows the geometric configuration of the test rig from the top view.

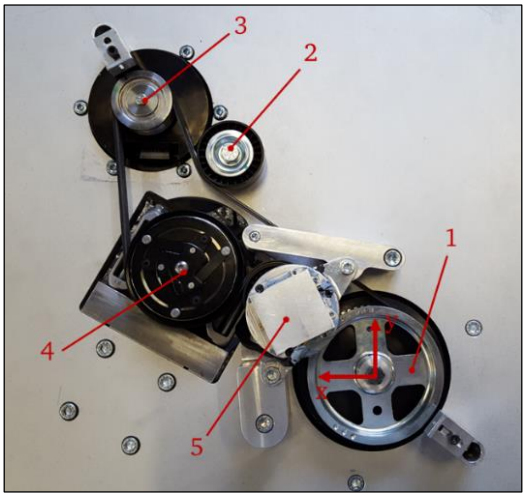

Figure 6 FEAD Layout

The layout reproduces the setup of a real engine front end, where the BDS connects five components: crankshaft, BSG, air conditioning compressor, automatic tensioner, idler pulley. The power in the belt drive is transmitted by a V-ribbed belt with 5 ribs. The layout was reproduced in a horizontal plane to have a uniform distribution of the forces acting on the frame and to avoid possible bending stresses on the bearing structure. The mounting solutions of the pulleys were adopted to allow the substitution of each pulley with others of different radii or coupled with belts of different number of ribs or type. The crankshaft (1) and BSG (3) pulleys were mounted on the shafts of two BoschRexroth IndraDyn H electric motors. The crankshaft is powered with motor MSS182D-0260 and the BSG with MSS102D-0800. Their specifications are listed in Table 1.

Table 1 Electric motors characteristics

Function	**Rated Speed** [rpm]	**Max Speed** [rpm]	**Rated Torque** [Nm]	**Max Torque** [Nm]	**Rated Power** [kW]	**Rated Current** [A]	**Max Current** [A]
Crankshaft	2600	12000	140	320	38.1	71	200
BSG	8000	22500	20	45	16.8	24	69

The frameless configuration of the two motors and their liquid cooling allowed to design their case to obtain a deep integration with the rest of the test rig. Two equal modular magnetic encoders ERM 2984 by Heidenhain (line count 192, $1V_{pp}$ sinusoidal incremental signals, maximum rotational speed $47000rpm$, power supply $5V_{dc}$) are mounted on the shafts to allow motor control and measure the angular position for acquisition purposes. The angular speeds of the crankshaft and BSG pulleys are additionally monitored by means of two optical tacho sensors. These devices employ a photoelectric sensor (OPB705 by Optek, power supply $5V_{dc}$) that detects the reflection of a line pattern printed onto the pulley surface. In order to measure the tension of the belt both in static and dynamic conditions the idler pulley (2) hub was instrumented with a load cell (DB-DA-750-17 by Magtrol, nominal force $750N$, power supply $5V_{dc}$). The AC compressor (4) was mounted as a unit in order to have the possibility to use it as a load, even though during the first experimental phase it will not be actuated and will behave just as an additional idler pulley. The automatic tensioner (5) installed on the test rig is a prototype that is able to adjust the belt tension in response to a software request input. The angular displacement of the tensioner's pivot is measured by means of a magnetic angle sensor module (KMA210 by NXP, angle resolution $0.04deg$, maximum angle $180deg$, external magnetic field strength $35kA/m$, power supply $5V_{dc}$).
Table 2 provides data on geometric and inertial characteristics of the components of the test rig.

Table 2 Parameters of accessories

Position	**Accessory**	**Pulley Diameter** [m]	**Coordinates** [X,Y] [m]	**Rotational Inertia** [kgm^2]
1	Crankshaft	126.0e-3	[0;0] e-3	53.4 e-3
2	Idler	65.0e-3	[136.2;216.0] e-3	24.6 e-6
3	BSG	54.0e-3	[220.4;269.0] e-3	4.5 e-3
4	AC Compressor	109.2e-3	[177.1;97.0] e-3	2.2 e-3
5	Automatic Tensioner	65.0e-3	[76.3;64.8] e-3	24.6 e-6

3.2. Sensors and actuators' system

The control architecture of the test rig is composed by a high voltage control section for the two electric motors and a low voltage ECU in charge of defining the reference speed to give as an input to the control loops of the two electric motors and of acquiring and analyzing the data read by the sensors mounted on the test rig.
The power supply (HMV01.1R-W0065-A-07 by BoschRexroth) powers both the inverters that are connected onto the same DC BUS. The main feature of such supply unit is the possibility of power regeneration at the mains, meaning that the power produced by one of the two motors acting as alternator

is given back to the network. The modular power section is completed by two BoschRexroth inverters, HMS01.1N-W0210 for Motor 1 and HMS01.1N-W0070 for Motor 2. The control sections (CSH01.1C-CO-ENS-EN2-MEM-L2-S) are the same for both inverters and provide three nested control loops: current, speed and position control. In the studied application the position control is not of interest, so such loop is not considered in the following analysis. The two inverters give the possibility of closing the control loops inside their firmwares but also outside by means of a dedicated control unit. The control laws implemented onto the inverters' firmware consist of a Proportional-Integral (PI) compensator for each control loop. It is possible to provide to each control loop a reference signal, in terms of position, speed or torque, via an external ECU through the master communication implementing the CANOpen Protocol. The two control sections allow the utilization of some optional features for analog and digital inputs and outputs, encoders acquisition, serial interface towards commissioning tool on PC, emulation of encoder data towards ECU, master communication with ECU through CANOpen Protocol.
The ECU is built around a Control Card based on a Texas Instruments floating point Digital Signal Processor (DSP). The Control Card is equipped with 16 ADC channels, capture and quadrature encoder modules and an asynchronous RAM which allows the real time acquisitions of the variables measured on the test rig by the sensors described above. Besides, the communication peripherals allow the use of the CANOpen protocol for communication towards the two inverters. The ECU is used to control the operations of the two motors, actuating the automatic belt tensioner and monitoring the parameters measured on the system.

4. TEST RIG CHARACTERIZATION

The sensors' layout of the test rig allows the monitoring of torque and speed conditions on both electric motors and can be used to evaluate the power losses of the system, identifying separately speed and torque losses.
The aim of the first analytical and experimental analysis was to obtain a preliminary characterization of the power losses that occur in the test rig. A particular effort was addressed to define a methodology to distinguish between losses due to test rig components and losses due to the belt drive system itself. The biggest portion of power loss of the test rig results from the inertia of the two electric motors, while a smaller part is linked to the inner losses of the motors and to those of the bearings mounted on the different components of the test rig. The reconfigurability of the test rig was exploited to perform the tests in different operating conditions in terms of belt preload. Different preload can be obtained both by setting the active tensioner in HI or LOW mode (to provide high or low belt pretension, respectively) and changing the position of one of the pulleys composing the BDS layout (in this case the position of the compressor pulley)therefore by elongating the belt.
Two critical issues involving the encoders of both electric motors affected the experimental tests in this first phase. On one side a bad calibration did not allow to run the motor attached to the crankshaft pulleyat its full speed range, on the other side a partial demagnetization prevented from running the BSG motor. Consequently, the first tests were not conducted exploiting the whole potentialities of the test rig but in those limited conditions that assured the data to be meaningful and valuable. In particular:

- BSG motor was used in idle condition
- Speed range of the motor on CS pulley is [0 – 3700] rpm
- AC compressor pulley clutch was decoupled

4.1. Crankshaft losses analysis

The first experiment involved the study of torque losses of the motor assembly on the crankshaft with no belt installed hence, no torque flow to other pulleys. The torque required by the motor to run the shaft at different constant speeds was obtained as feedback on the inverter.
In Fig 7 the red stars corresponds to the crankshaft torque profile at different speed determined experimentally. The measured torque values include the torque required to overcome the shaft's inertia, the inner losses of the electric motor and the bearing losses due to axial loads. Radial loads on the bearings were equal to zero because of the absence of the belt.
The same study is expected to be done on the BSG motor to evaluate its inner losses.

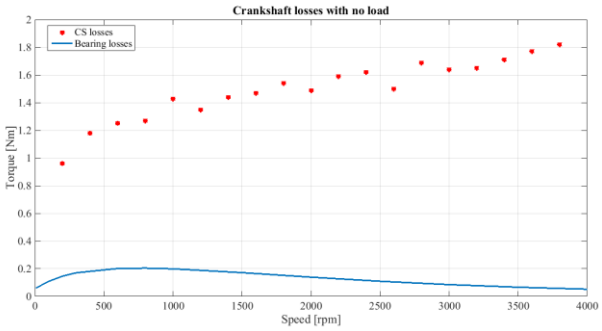

Figure 7 Measured torque losses on the crankshaft with no load and calculated bearing losses due to two radial ball bearings supporting the crankshaft motor assembly

4.2. Bearing losses analysis

The bearing losses were calculated using the method implemented by SKF® and were performed for each individual bearing installed in the test rig. All the used bearings are single row deep groove ball bearings capped on both sides with an internal lubrication. The amount of friction torque in a rolling bearing depends on the applied loads and other factors such as operating speed, bearing type/size and lubrication. The model developed by SKF® to calculate the friction and power losses follows the real behavior of the bearing as it takes the internal and external influences into account and therefore can be considered reliable [16].

The overall torque loss due to bearings results in a peak value of torque around 600Nmm at low speeds and high pretensions. An order of calculated torque loss on the sole crankshaft assembly and the measured values of overall torque loss are shown in Fig 7. The bearing losses are represented as the blue line and they result negligible amount in comparison to the overall losses of the system.

4.3. Speed and torque losses

Eventually tests to identify speed and torque losses were performed on the complete system at constant speeds for different tension conditions. The torque produced by the crankshaft motor and the speed transmitted to the BSG pulley were monitored to measure the overall torque and speed losses of the BDS.

The overall speed loss is given by the sum of the different contributions described in Section 2 and can be analytically expressed as:

$$\%\text{overall speed loss} = \frac{\omega_{\text{driver}} - \eta\omega_{\text{driven}}}{\omega_{\text{driver}}} \times 100 \qquad (2)$$

Where: ω_{driver} - measured speed of driving motor shaft, i.e. crankshaft motor; ω_{driven} - measured speed of driven motor shaft, i.e. BSG motor; η - transmission ratio.

Figure 8 shows the measured speed loss over the belt pretension for different crankshaft constant speeds. Black and blue lines identify respectively LOW and HI tension modes of the tensioner. The experimental data showed that for no load operating condition, the speed loss decreases with a belt pretension increase while varying crankshaft speeds does not affect significantly the overall speed losses.

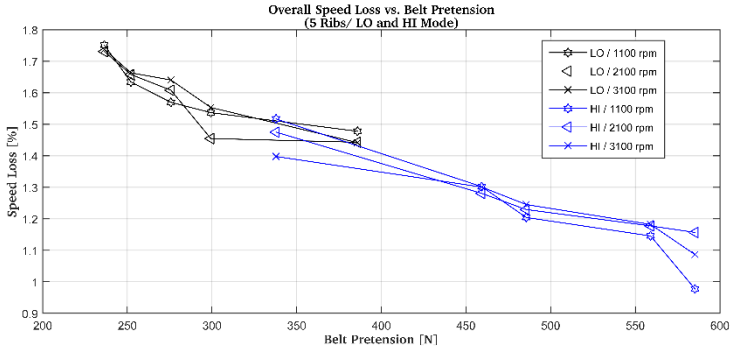

Figure 8 Overall speed losses over belt pretension at different speed values

In the preliminary tests, the influence of belt pretension on overall torque losses was not taken into account. Instead, the test were focused on the influence of crankshaft speed variations. The reason for this was that the tests were done with no load on the BDS (alternator and AC compressor idling), as highlighted before. This condition does not replicate realistic behavior of the BDS on engine regarding torque losses, as BDS mainly works in loaded (even with partial load) conditions. To distinguish the hysteresis behavior in the overall torque loss, progressive measurements were done with 2, 3, 4 and 5 ribs belts. One rib belt (or only belt reinforcement cord) could give better insight on torque losses due to bearings and inner losses in the BDS components. But due to issues related to misalignment and proper tensioning of the belt in this case, it was omitted. The results shown in Figure 9 highlight that torque losses increase with increasing speed and increasing number of ribs, which extends the contact surface between belt and pulleys.

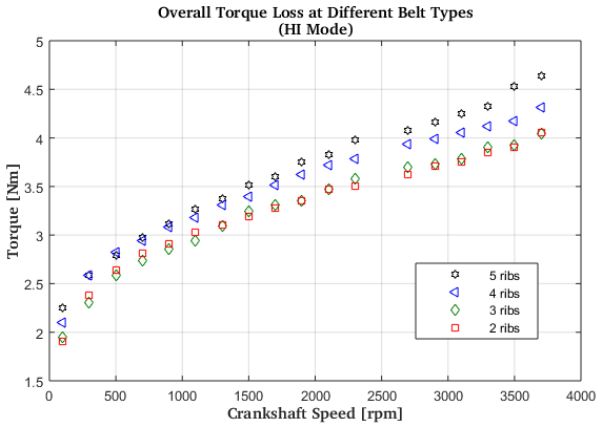

Figure 9 Torque losses for different belt width

4.4. Overall power losses

Figure 10 summarizes the experimental analysis that was conducted on a belt drive system using a 5 ribs belt to transmit power to the accessories. The composition of torque and speed losses results in an overall power loss that increases with increasing crankshaft speeds and is constant over pretension for no load condition of operation. These result identify the torque losses as the main contribution to power losses in stationary conditions, as stated by [12].

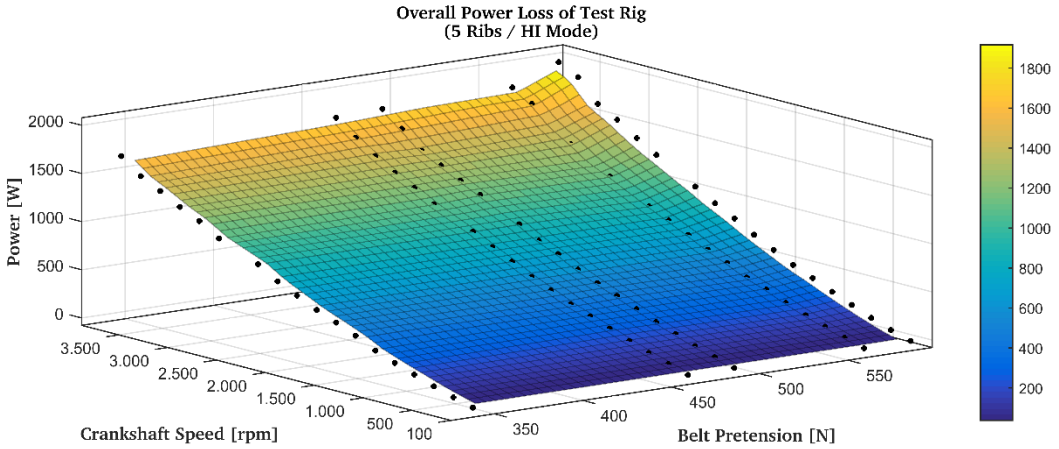

Figure 10 Overall power loss obtained on test rig for increasing values of crankshaft speed and belt pretension

5. CONCLUSIONS

The present work provides an exhaustive description of the critical issues that can arise over the different operating conditions of a BDS equipped with a BSG. A test rig was designed and realized for the

experimental analysis and characterization of power losses for front end accessory drives into automotive applications. The preliminary experimental tests performed a progressive analysis of the different contributions to the overall power losses into the test rig: electric motor losses, bearing losses speed and torque losses of the BDS. The test rig characterization is still in progress, especially for what concerns the BSG electric motor losses characterization. Future experiments will contemplate tests at constant speed imposed by the CS with varying torque requests from the BSG aimed at the characterization of the slip phenomena at the contact surfaces of the pulleys and the power dissipation evaluation of the BDS. Additional tests in dynamic conditions will be performed, simulating real operating conditions of crankshaft and BSG, for the evaluation of the natural frequencies of the transmission.

BIBLIOGRAPHY

[1] Bojoi, Radu, et al. "Multiphase starter generator for 48V mini-hybrid powertrain: Design and testing." Power Electronics, Electrical Drives, Automation and Motion (SPEEDAM), 2014 International Symposium on. IEEE, 2014.

[2] Walters, James E., et al. Technology considerations for belt alternator starter systems. No. 2004-01-0566. SAE Technical Paper, 2004.

[3] Arnold, Ing Manfred, and Dipl Ing Mohamad El-Mahmoud. "A Belt-Driven Starter-Generator Concept for a 4-Cylinder Gasoline Engine." AutoTechnology3.3 (2003): 64-67.

[4] G. Cariccia and D. Licata, "Actuated tensioner for an accessory drive". Patent WO2013190524 A1, 2013.

[5] G. Genta and L. Morello, "The automotive chassis. Volume 2: System design", 2009.

[6] B. G. Gerbert "Power Loss and Optimum Tensioning of V-Belt Drives," J. Eng. for Industry, vol. 96, no. 3, p. 877, 1974.

[7] T. H. C. Childs and D. Cowburn, "Power transmission losses in V-belt drives Part 1: Mis-matched belt and pulley groove wedge angle effects," ARCHIVE: Proceedings of the Institution of Mechanical Engineers, Part D: Transport Engineering 1984-1988 (vols 198-202), vol. 201, no. 14, pp. 33–40, 1987.

[8] T. H. C. Childs and D. Cowburn, "Power transmission losses in V-belt drives Part 2: Effects of small pulley radii," ARCHIVE: Proceedings of the Institution of Mechanical Engineers, Part D: Transport Engineering 1984-1988 (vols 198-202), vol. 201, no. 14, pp. 41–53, 1987.

[9] T. F. Chen and C. K. Sung, "Design considerations for improving transmission efficiency of the rubber V-belt CVT," IJVD, vol. 24, no. 4, p. 320, 2000.

[10] T. F. Chen, D. W. Lee, and C. K. Sung, "An experimental study on transmission efficiency of a rubber V-belt CVT," Mechanism and Machine Theory, vol. 33, no. 4, pp. 351–363, 1998.

[11] G. Gerbert, "Belt Slip—A Unified Approach," J. Mech. Des, vol. 118, no. 3, p. 432, 1996.

[12] D. G. Alciatore, "Multipulley belt drive mechanics: Creep theory vs. shear theory", 1987.

[13] G. Čepon, L. Manin, and M. Boltežar, "Validation of a flexible multibody belt-drive model," Strojniški vestnik.

[14] B. G. Gerbert, "Force and slip behaviour in V-belt drives". Helsinki: Finnish Academy of Technical Sciences, 1972.

[15] L. Bertini, L. Carmignani, and F. Frendo, "Analytical model for the power losses in rubber V-belt continuously variable transmission (CVT)," Mechanism and Machine Theory, vol. 78, pp. 289–306, 2014.

[16] SKF Group, Rolling bearings catalogue, 2013.